Article

Oxidation Behavior of Carbon Fibers in Ceramizable Phenolic Resin Matrix Composites at Elevated Temperatures

Tingli Yang, Chuang Dong, Yiyang Rong, Zongyi Deng, Pengfei Li, Pengkun Han, Minxian Shi * and Zhixiong Huang

Key Lab of Advanced Technology for Specially Functional Materials, Ministry of Education, School of Materials Science and Engineering, Wuhan University of Technology, Wuhan 430070, China; 257416@whut.edu.cn (T.Y.); dongchuang@whut.edu.cn (C.D.); rongyiyang0808@163.com (Y.R.); zong_yi_deng@whut.edu.cn (Z.D.); 303773@whut.edu.cn (P.L.); hpk051157@whut.edu.cn (P.H.); zhixiongh@whut.edu.cn (Z.H.)
* Correspondence: minxianshi@whut.edu.cn

Abstract: Carbon fiber fabric-reinforced phenolic resin composites are widely used as thermal protection materials for thermal protection systems in hypersonic vehicles and capsules. In this work, carbon fiber fabric-reinforced boron phenolic resin composites modified with $MoSi_2$ and B_4C were prepared via a compression molding technique. The high-temperature performance of the composites as well as the oxidation behavior of the carbon fibers was studied. The results indicate that the incorporation of B_4C improves the performance of composites at high temperatures. The residual weight rate of composites with 15 phr B_4C (BP-15) sufficiently increased from 23.03% to 32.91% compared with the composites without B_4C (BP-0). After being treated at 1400 °C for 15 min, the flexural strength of BP-15 increased by 17.79% compared with BP-0. Compared with BP-0, the line ablation rate and mass ablation rate of BP-15 were reduced by 53.96% and 1.56%, respectively. In addition, $MoSi_2$ and B_4C particles had a positive effect on the oxidation of carbon fibers in the composites. After treatment at 1400 °C, the diameter of the as-received carbon fiber was reduced by 31.68%, while the diameter of the carbon fiber in BP-0 and BP-15 decreased by 15.12% and 6.14%, respectively. At high temperatures, the liquid B_2O_3 from B_4C and $MoSi_2$-derived complex-phase ceramics (MoB, MoB_2, Mo_2C, $Mo_{4.8}Si_3C_{0.6}$) acted as an oxygen barrier, effectively mitigating the oxidation degree of the carbon fibers.

Keywords: carbon fiber; oxidation; ceramizable; polymer–matrix composites; high-temperature properties; ablation

1. Introduction

During hypersonic flight in the atmosphere, the thermal load transmitted to a spacecraft due to the phenomenon of aerodynamic heating has a serious impact on the operation of the instruments in the cabin and jeopardizes the safety of the spacecraft [1]. As a result, a thermal protection system (TPS) must be installed on the surface of the spacecraft to prevent heat from entering the interior of the cabin and ensure the spacecraft's normal operation. Common thermal protection is generally achieved by use of a heat sink, ablation, and radiation, of which ablative thermal protection is the safest and most cost-effective thermal protection scheme. Ablative materials achieve thermal protection through their own ablation processes. On the one hand, physical and chemical changes such as melting, decomposition, and sublimation occur in ablated materials at high temperatures, which causes a large amount of heat to be dissipated. On the other hand, the carbon layer formed by the cracking of the material surface can further prevent heat transfer to the interior of the material [2,3].

Fiber-reinforced resin matrix composites with designability and simple processes have been used in different industries, especially in the field of ablative thermal protection materials. Among a variety of resin matrix materials, phenolic ablation materials are widely used as ablation materials because of their excellent heat resistance and thermal stability [4]. However,

phenolic resin is brittle and easy to crack at high temperatures, forming a loose and porous carbon layer that further accelerates the oxidative cracking of the internal structure and reduces the residual strength of the material [5]. In order to improve the performance of phenolic materials in high-temperature applications, phenolic resins are modified by adding ceramic fillers to obtain ceramizable composites, which allows the material to be molded at low temperatures and exhibit excellent properties at high temperatures. The introduction of ceramic fillers leads to the ceramizable reaction of composites at high temperatures, and the formation of dense ceramic structure on the surface plays a role in thermal oxygen resistance, which improves the high-temperature performance of composites. Aqeel Saghar et al. [6] demonstrated that the ablation rate of hybrid carbon fiber phenolic matrix composites with 5 wt% silicon carbide added was reduced to 33%. Shuang Wang et al. [7] explained that the introduction of silicon carbide particles effectively improved the mechanical properties, thermal properties, and ablation resistance of carbon–phenolic (C/Ph) composites. Jiuqiang Song et al. [8] found that the addition of $ZrSi_2$ increased the initial decomposition temperature of the silicone rubber composites and reduced the linear and mass ablation rates. Yaxi Chen et al. [9] found that the method of introducing zirconium diboride particles could significantly improve the ablation resistance and insulation performance of C-Ph composites. Jie Ding et al. [10] showed that the addition of titanium diboride enhanced the thermal stability of the phenolic resin and the mechanical performance of carbon–phenolic composites at high temperature. Feng Xu et al. [11] found that $TaSi_2/ZrSi_2$ modified carbon–phenolic composites possessed a good resistance to long-term laser ablation. Wei Yang et al. [12] revealed that the addition of $MoSi_2$ reduced the linear and the mass ablation rate of composites by about 94.46% and 39.09%. Among them, $MoSi_2$ had excellent oxidation resistance at high temperatures. JianHui Yan et al. [13] prepared a protective $MoSi_2$ coating on a Nb substrate, which exhibited excellent oxidation resistance in air at 1200 °C. However, when the temperature was lower than 800 °C, the creep resistance of $MoSi_2$ became poor and insect degradation occurred [14]. As the temperature increased, the oxidation resistance of $MoSi_2$ increased [15–17]. The introduction of B_4C has been found to effectively improve the oxidation resistance of $MoSi_2$ at relatively low temperatures. Ping Zhang et al. [18] prepared $MoSi_2$-B_4C coatings on Nb alloy via a spark plasma sintering (SPS) process. His work found that the $MoSi_2$-B_4C coating showed better oxidation resistance at 1450 °C compared to the single-layer $MoSi_2$ coating.

Carbon fiber is widely used as a reinforcement fiber in thermal protection ablation materials, as it has low density (1.7–2.0 g/cm^3), high strength, high modulus (tensile strength 3–7 GPa, tensile modulus 200–650 GPa), a low thermal expansion coefficient (0–1.1 $\times$ 10^{-6}/K), high thermal conductivity (10–160 W/m·K) and other excellent performance [19–22]. Carbon fiber can still maintain good mechanical properties in an inert atmosphere above 2000 °C. However, it is easily oxidized under a high-temperature aerobic environment, which greatly weakens its comprehensive mechanical properties, and the stability of the composites declines sharply [23,24]. Gyungha Kim et al. [25] explored the mechanical properties of carbon fibers after heat treatment in nitrogen and oxygen atmospheres. They found that the tensile strength at 500 °C was equivalent to that of the virgin carbon fibers in the nitrogen atmosphere, decreasing to 71% at 1000 °C. In the oxygen atmosphere, the tensile properties gradually decreased at 500 °C and the carbon fibers deteriorated above 600 °C, at which point the tensile properties were unable to be measured. Therefore, solving the oxidation problem is the key to the use of carbon fiber-reinforced composites for high temperatures [26–28]. Feng Xu et al. [29] prepared $ZrSiO_4$ sol and sprayed it on carbon fiber fabrics, improving the interfacial properties and the ablation resistance of the composites. Liuyang Duan et al. [30] introduced polycarbosilane (PCS) as an interface layer onto carbon fiber, which effectively improved the performance of carbon fiber-reinforced phenolic resin composites (CPR) at high temperatures. Zhenyue Zou et al. [31] showed that ZrO_{2f}-coated C_f hybrid fibrous reinforcements exhibited good thermal stability and high oxidation resistance. Guangyuan Yang et al. [32] proposed two kinds of carbon fibers with antioxidant coating, which were used as reinforcement components to prepare phenolic resin matrix composites. The results showed that both

SiC/SiO$_2$ coated carbon fibers and SiC-ZrO$_2$-MoSi$_2$/Ni coated carbon fibers improved the oxidation resistance of the composites without reducing the mechanical properties of the composites, with the failure temperature at around 1200 °C to 1600 °C.

Many studies have shown that the interface modification between fibers and substrates as well as the introduction of fillers have a positive effect on the high-temperature performance of composites. However, little attention has been devoted to the oxidation behavior of carbon fibers in ceramizable composites. Therefore, the purpose of this work is to study the performance of ceramizable composites and the oxidation behavior of carbon fibers in ceramizable composites at high temperatures. Carbon fiber fabric-reinforced boron phenolic resin composites modified by MoSi$_2$ and B$_4$C were prepared via a compression molding technique. The micromorphology of both the carbon fibers and the composites as well as the phase composition, thermal stability, flexural strength, and ablation resistance of the composites were characterized. This provides theoretical guidance for further research on the performance of carbon fiber and its composites in high-temperature environments.

2. Experimental

2.1. Raw Materials

Carbon fiber fabric (W-7022FF-400, Weihai Guangwei Composite Materials Co., Ltd., Weihai, China) was used for the reinforcement of composites while boron phenolic resin (THC-400, Shaanxi Taihang Fire Resistant Polymer Co., Ltd., Xian, China) was used as the matrix. MoSi$_2$ with a particle size of 1 μm, used as filler, was supplied by Shanghai Buwei Applied Materials Technology Co., Ltd., China while B$_4$C with a particle size of 1–10 μm, used as a fluxing agent, was obtained from Shanghai Aladdin Bio-Chem Technology Co., Ltd., Shanghai, China. Absolute ethanol (analytically pure, Sinopharm Chemical Reagent Co., Ltd., Ningbo, China) was used as a solvent. All materials were used as-received without further purification.

2.2. Preparation of Composites

The preparation of composites followed the following procedures (Figure 1). Firstly, boron phenolic resin powder was dissolved in an equal mass of ethanol at 80 °C for 4 h. Then, MoSi$_2$ and B$_4$C particles were introduced into boron phenolic resin solution according to the formula in Table 1 and mechanically stirred for 1 h at a speed of 600 rpm to obtain a uniformly mixed ceramizable boron phenolic resin solution. Next, the ceramizable boron phenolic resin solution was coated onto carbon fiber fabric to prepare prepregs with the mass ratio of carbon fiber fabric to solution being 1:2.5. The prepregs were dried for 48 h at 35 °C to sufficiently evaporate the ethanol before being piled. Finally, the piled prepregs were put into a mold and cured in a plate vulcanizing machine via a compression molding technique to obtain ceramizable composites [33].
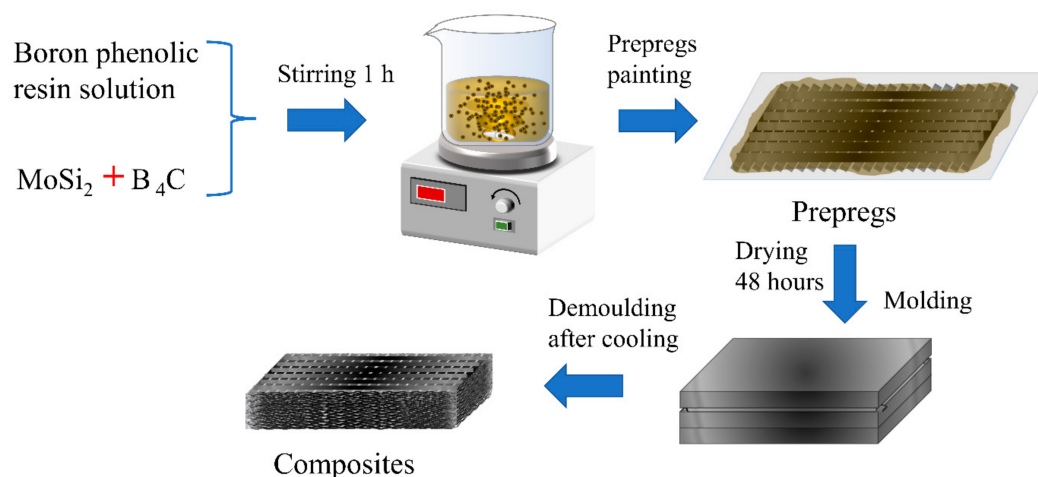

Figure 1. Preparation process of composites.

Table 1. Formula of ceramizable boron phenolic resin solution.

Samples	Boron Phenolic Resin Solution (phr)	$MoSi_2$ (phr)	B_4C (phr)
BP-0	100	65	0
BP-5	100	65	5
BP-10	100	65	10
BP-15	100	65	15
BP-20	100	65	20

2.3. Thermal Oxidation Treatment of Carbon Fibers and Composites

The as-received carbon fiber fabric was treated in an air atmosphere in a muffle furnace for 15 min. The temperatures were 800 °C, 1000 °C, 1200 °C, and 1400 °C, respectively. The same went for flexural strength test samples before being tested in a universal testing machine.

2.4. Characterizations

A scanning electron microscope (JSM-7500F, Tokyo, Japan) was used to observe the microscopic morphology and elemental composition of samples after high-temperature oxidation treatment. After high-temperature treatment, the composites were subjected to phase analysis using an X-ray diffractometer (D/MAX-RB, The Hague, The Netherlands) at a scan rate of 10°/min. The thermal stability of the carbon fibers and composites was characterized using an integrated thermal analyzer (STA449F3) from room temperature to 1450 °C with a heating rate of 10 °C/min. The density of the composites was tested using the Archimedes method. The flexural strength of composites was tested via a universal testing machine (RGM4100, Chengdu, China) according to the Chinese recommended standard GB/T 1449-2005. The functional groups of the carbon fibers were recorded using a Fourier transform infrared spectrometer (Nexus, Gaithersburg, MD, USA) in the range of 4000 to 500 cm^{-1} while the degree of graphitization was calculated based on the Raman spectra recorded using a Raman microprobe (InVia, Wotton under Edge, UK). The ablation performance of the composites was measured under an oxygen–acetylene torch according to the Chinese standard GJB 323A-96. The line ablation rate and mass ablation rate were calculated based on the following formulas:

$$\text{Line ablation rate} = \frac{\Delta l}{\Delta t} \tag{1}$$

$$\text{Mass ablation rate} = \frac{\Delta m}{\Delta t} \tag{2}$$

where Δl and Δm represent the change in thickness and the mass loss of samples, respectively, and Δt stands for change in time.

3. Results and Discussion

3.1. Thermal Stability of Carbon Fibers and Composites

Thermogravimetric analysis was used to analyze the thermal stability of the carbon fibers and composites in nitrogen and air atmospheres, as shown in Figure 2. There was no obvious weight change in the carbon fibers in the nitrogen atmosphere. The slight peak at around 60 °C in the DTG curve in the nitrogen atmosphere was attributed to desorption of absorbed air and water. However, the weight loss increased significantly from 600 °C to 1000 °C in the air atmosphere, and we noted an obvious peak at around 900 °C. The final residue yield was only around 15% above 1000 °C, which was much different from that of carbon fibers in the nitrogen atmosphere. The above-mentioned results show that carbon fibers are easy oxidize above 600 °C in an air atmosphere.
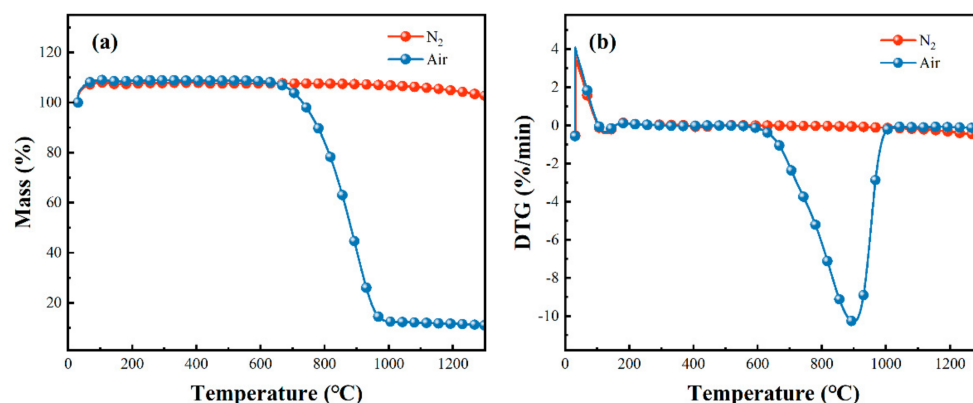
Figure 2. TG curve (**a**) and DTG curve (**b**) of carbon fibers in nitrogen and air atmospheres.

Figure 3 shows the TG and DTG curves of $MoSi_2$ particle-modified boron phenolic resin composites with different contents of B_4C particles in an air atmosphere. The slight weight loss below 200 °C was mainly caused by volatilization of absorbed water while that at 200 °C to 400 °C was mainly due to further dehydration reaction of the residual aldehydes and phenolic monomers in the boron phenolic resin [34]. The strong peaks in the DTG curve at around 750 °C to 900 °C were induced by the violent pyrolysis of resin to produce gases such as CO, CO_2, C_2H_6, H_2O, etc. [35,36]. The residue yields at 1400 °C were 24.03%, 28.36%, 30.22%, 32.91%, and 30.02%, respectively. It is obvious that the residue yield went high with the increase in contents of B_4C particles but decreased slightly when the content of B_4C reached 20 phr. The main reason is that B_4C react with oxygen at elevated temperatures to produce B_2O_3, which is a weight-gaining reaction. However, B_2O_3 is easy to volatilize at elevated temperatures, which is a weight-decreasing process. Additionally, the DTG curve and Table 2 show that the greater the content of B_4C particles, the higher the temperature when the maximum pyrolysis reaction rate is reached. Therefore, 15 phr B_4C can efficiently increase the thermal stability and residue yield of composites.
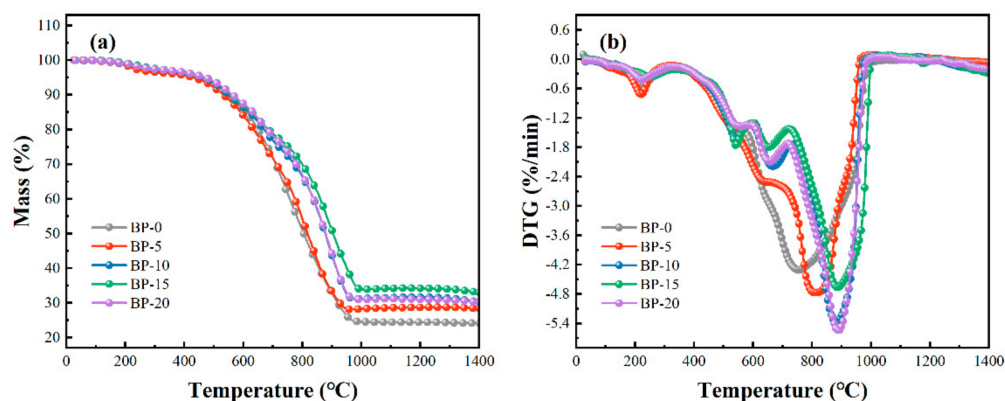

Figure 3. TG curve (**a**) and DTG curve (**b**) of $MoSi_2$ particles modified boron phenolic resin composites with different contents of B_4C particles in air atmosphere.

Table 2. Thermal decomposition characteristics of composites.

Samples	[1] Tmax/°C	Residue Yield/%		
		500 °C	1000 °C	1400 °C
BP-0	755.2	93.20	50.78	24.03
BP-5	813.4	92.11	54.02	28.36
BP-10	885.0	93.44	66.31	30.22
BP-15	886.0	93.93	69.92	32.91
BP-20	892.4	93.79	66.65	30.02

[1]: Tmax is the temperature at which the rate of thermal weight loss is maximum.

3.2. Flexural Strength of Composites Treated at Different Temperatures

The influence of B_4C particulate content on the flexural strength of composites was studied, as shown in Figure 4. After being treated at 800 °C for 15 min, the flexural strength of BP-0 was 68.79 MPa, which increased with increasing B_4C particles within a certain range. The flexural strength reached its maximum value of 81.91 MPa when 15 phr of B_4C particles were added; however, it decreased to 77.65 MPa when 20 phr of B_4C particles were added. The flexural strength dropped with increasing the temperature to 1000 °C and 1200 °C. However, the flexural strength increased abnormally when the temperature was further increased to 1400 °C. To be specific, the flexural strength of BP-0 was 61.58 MPa after being treated at 1400 °C for 15 min, which was much higher than that from being treated at 1000 °C and 1200 °C. Similarly, the same trend is observable for composites with B_4C particles ranging from 5 phr to 20 phr.
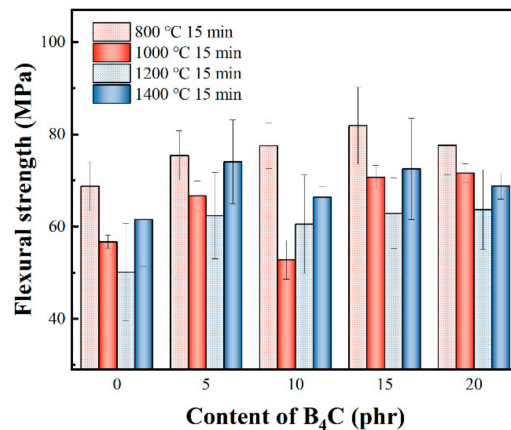

Figure 4. Flexural strength of composites with different contents of B_4C after treatment at different temperatures.

3.3. Micromorphology Changes of Composites with Different Contents of B_4C

To figure out the reasons for this evolution of flexural strength, SEM analysis was conducted on the surface of the composites after treatment at different temperatures. As shown in Figure 5 and Table 3, the diameter of the carbon fibers exposed for both BP-0 and BP-15 dropped with increasing temperature, ranging from 800 °C to 1200 °C. However, the diameter of carbon fibers in the composites treated at 1400 °C was slightly smaller than that of those treated at 800 °C and much bigger than that of those treated at 1000 °C and 1200 °C. The above findings are consistent with the evolution of flexural strength. That is to say, the carbon fibers in composites treated at 1400 °C were less oxidized than those treated at 1000 °C and 1200 °C, which is incredible.
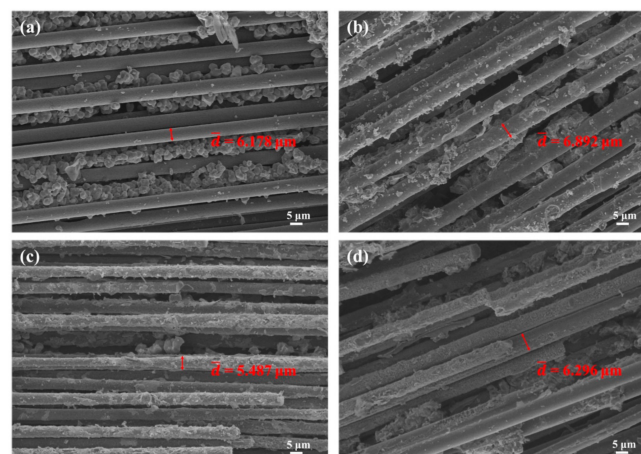

Figure 5. *Cont.*
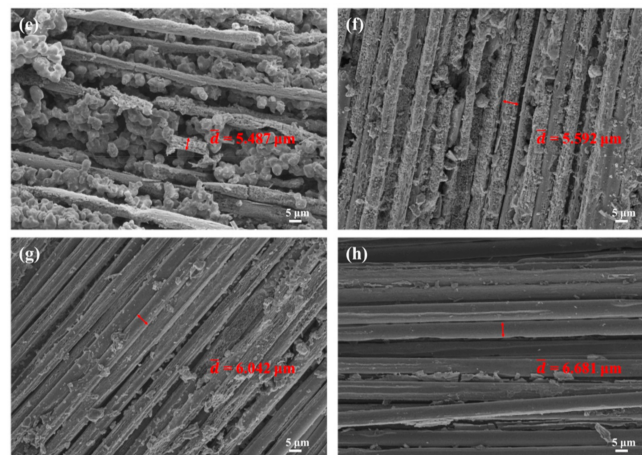
Figure 5. Micromorphology of BP-0 and BP-15 treated at different temperatures for 15 min: BP-0 at (**a**) 800 °C, (**c**) 1000 °C, (**e**) 1200 °C, and (**g**) 1400 °C; BP-15 at (**b**) 800 °C, (**d**) 1000 °C, (**f**) 1200 °C, and (**h**) 1400 °C.

Table 3. Diameter changes of carbon fibers treated at different temperatures.

Treatment Temperature	$\overline{d}/\mu m$		
	Carbon Fibers	**BP-0**	**BP-15**
RT	7.118	7.118	7.118
800 °C	6.034	6.178	6.892
1000 °C	5.393	5.487	6.296
1200 °C	4.999	5.097	5.592
1400 °C	4.863	6.042	6.681

3.4. Phase Evolution of Composites at Elevated Temperatures

To further find out the reasons for the diameter changes in the composites and explore the phase evolution of composites at elevated temperatures, the composites were subjected to phase analysis after high-temperature treatment. It can be seen from Figure 6 that the main component of both BP-0 and BP-15 at temperatures ranging from room temperature to 1400 °C was $MoSi_2$, which indicates that the $MoSi_2$ in the composites was relatively stable while the boron phenolic resin itself pyrolyzed intensely at high temperatures.
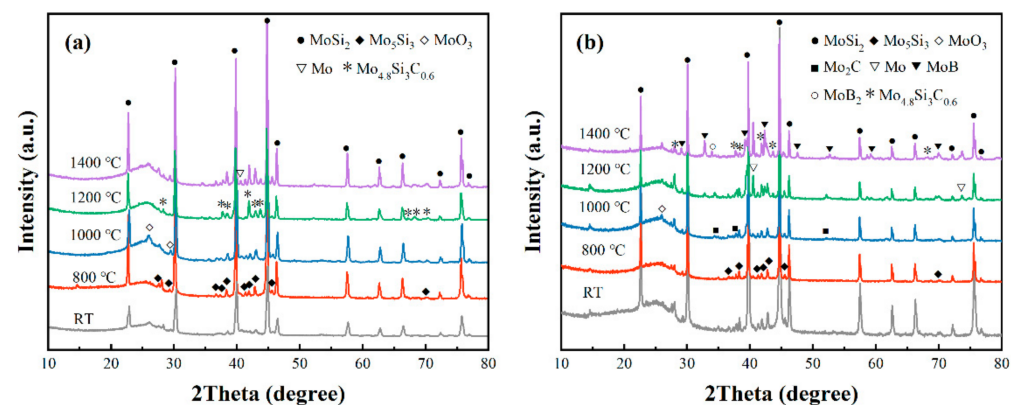

Figure 6. XRD patterns of the residue phases of BP-0 (**a**) and BP-15 (**b**) at different temperatures.

When the temperature reached 800 °C, a small amount of $MoSi_2$ reacted with oxygen to produce Mo_5Si_3 and amorphous SiO_2 [37,38]. However, due to its amorphous state, no obvious SiO_2 peak was detected.

$$5MoSi_2 + 7O_2(g) = Mo_5Si_3 + 7SiO_2 \tag{3}$$

After being treated at 1000 °C, it can be seen in the XRD patterns that the MoO_3 phase appeared in both BP-0 and BP-15, which was due to the selective oxidation of $MoSi_2$. Moreover, MoO_3 reacted with pyrolytic carbon to form carbides, so the Mo_2C phase could be found in BP-15.

$$MoSi_2 + 3.5O_2(g) = MoO_3 + 2SiO_2 \tag{4}$$

$$2MoO_3 + 7C = Mo_2C + 6CO(g) \tag{5}$$
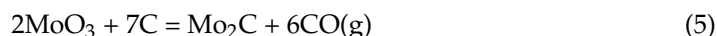
In the XRD pattern of BP-0 at 1200 °C, the $Mo_{4.8}Si_3C_{0.6}$ crystal phase was identified; it is possible that it was generated from the reaction of $MoSi_2$ with pyrolytic carbon in an air atmosphere [39–41]. At the same temperature, the characteristic peaks of Mo were found in the XRD pattern of BP-15, which may be attributed to the reaction of MoO_3 with pyrolytic carbon as well.

$$4.8MoSi_2 + 0.6C + 6.6O_2(g) = Mo_{4.8}Si_3C_{0.6} + 6.6SiO_2 \tag{6}$$

$$MoO_3 + 3C = Mo + 3CO(g) \tag{7}$$

As the treatment temperature increased to 1400 °C, characteristic peaks of Mo were found in the XRD patterns of BP-0, while $Mo_{4.8}Si_3C_{0.6}$, MoB and MoB_2 phases were identified in the XRD patterns of BP-15. The occurrence of borides was attributed to the addition of B_4C. The equations of the chemical reactions involved are as follows [18,42].

$$MoO_3 + 0.25B_4C + 2.75C = MoB + 3CO(g) \tag{8}$$

$$MoO_3 + 0.5B_4C + 2.5C = MoB_2 + 3CO(g) \tag{9}$$
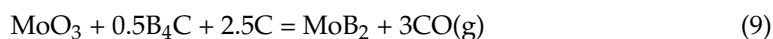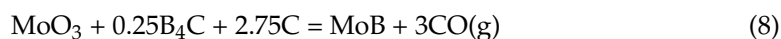
3.5. Micromorphology Changes and Phase Evolution of Carbon Fibers Treated at Different Temperatures

To further confirm the positive effect of $MoSi_2$ and B_4C on carbon fiber anti-oxidation, as-received carbon fibers were treated the same as composites and acted as a blank comparison. The treated carbon fibers were characterized using SEM, FT-IR and Raman spectra.

Figure 7 shows the changes in the surface morphology of carbon fibers treated at different temperatures. As shown in Figure 7 and Table 3, the diameter of the carbon fibers decreased with increasing treatment temperatures. To be specific, the diameter of carbon fibers at room temperature was about 7.118 μm, decreasing sharply to 4.863 μm after being treated at 1400 °C for 15 min. Obviously, the carbon fibers reacted with oxygen to form CO and/or CO_2, leading to the decrease in diameter of the carbon fibers.

FT-IR was used to observe the functional group changes before and after being treated at different temperatures. As shown in Figure 8, the peak attributed to -OH stretching vibration at ~3433 cm^{-1} and the peak associated with C=O stretching vibration at ~1624 cm^{-1} were enhanced with increasing treatment temperatures. The above results indicate that the degree of oxidation of carbon fibers deepened with increasing treatment temperatures, which is consistent with the SEM results.
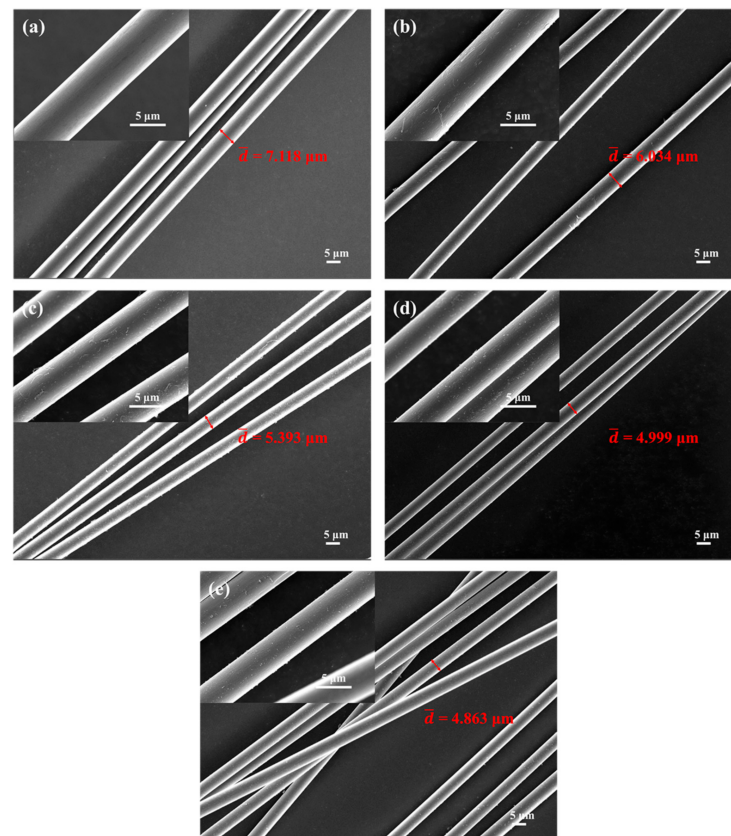
Figure 7. Micromorphology of carbon fibers treated at different temperatures for 15 min: (**a**) room temperature, (**b**) 800 °C, (**c**) 1000 °C, (**d**) 1200 °C, and (**e**) 1400 °C.
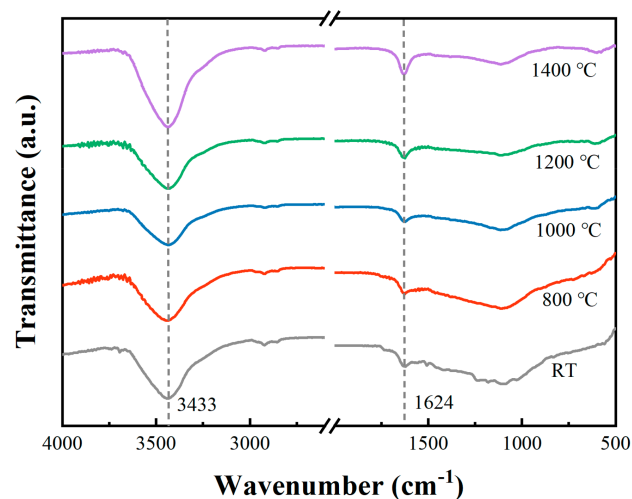

Figure 8. FT-IR spectra of carbon fibers.

Meanwhile, Raman spectra were used to identify the degree of graphitization of the carbon fibers before and after being treated at 1400 °C (Figure 9). After being oxidized in air at 1400 °C for 15 min, the calculated R value increased from 1.59 to 1.68, indicating that the degree of graphitization decreased after treated at 1400 °C. Raman spectra further confirmed that the degree of oxidation of the carbon fibers deepened as well.
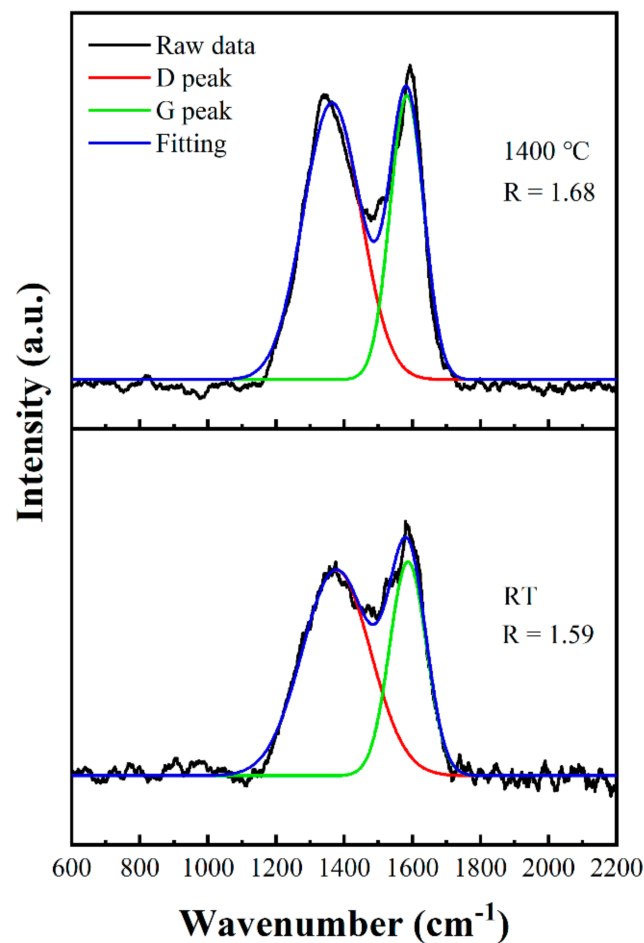
Figure 9. Raman spectra of carbon fibers.

3.6. The Ablation Behavior of Composites

3.6.1. The Ablation Properties of Composites under an Oxygen–Acetylene Torch

As shown in Figure 10, the linear ablation rate of the composites decreased markedly with increasing B_4C particles. To be specific, the linear ablation rate was 0.0424 mm/s without B_4C particles, dropping sharply to 0.013 mm/s with 20 phr B_4C particles. However, this was not the case for the mass ablation rate. The mass ablation rate was 0.0828 g/s without B_4C particles, decreasing smoothly with increasing B_4C particles within a certain range. The mass ablation rate reached its minimum value of 0.0815 g/s with 15 phr B_4C particles before it went high to 0.0840 g/s with 20 phr B_4C particles. Two factors may account for this. On the one hand, as described in 3.1, the oxidation reaction of B_4C is a weight gain reaction while the volatilization of B_2O_3 is a weight loss process. On the other hand, the melting temperature of B_2O_3 is only about 450 °C. Therefore the molten B_2O_3 can easily be washed away from the surface of a composite under an oxygen-acetylene torch with temperatures up to 1900 °C and high velocity airflow, this being a weight loss process as well [43–46]. Therefore, a compromise between weight-gaining reactions and weight loss processes was reached with 15 phr B_4C particles, leading to the minimum mass ablation rate. When the B_4C content increased to 20 phr, more molten B_2O_3 was generated on the surface of the composite. However, due to the oxyacetylene torch, a large amount of molten B_2O_3 was washed away from the composite surface, far exceeding the amount of oxidation weight gain of B_4C, resulting in a high mass ablation rate.
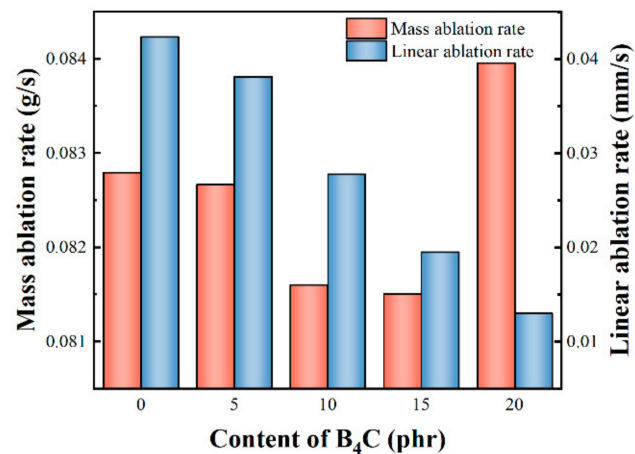
Figure 10. Mass ablation rate and linear ablation rate of composites.

3.6.2. Morphology of Ablated Surface

Figure 11 shows the macroscopic morphology of the composites after oxygen–acetylene ablation. It can be seen that there was an obvious pit in the middle of BP-0 after being ablated that shallowed gradually with increasing B_4C particles, which is consistent with the previous linear ablation rate results. In addition, a white substance occurred and increased on the outer ring of the ablated surface with increasing B_4C particles.
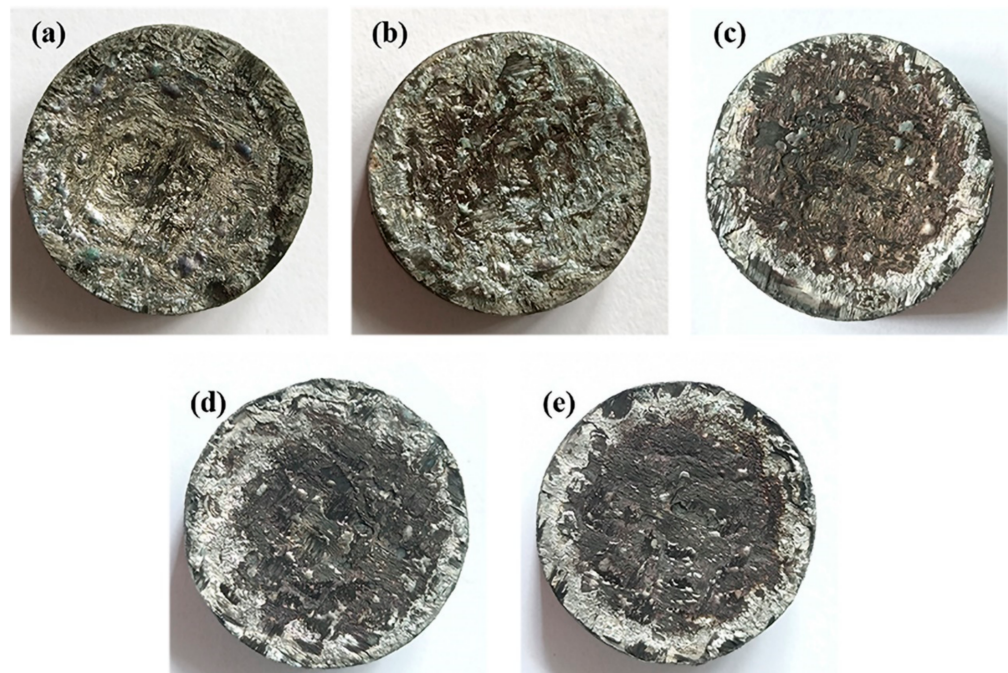

Figure 11. Macroscopic morphology of composites after oxygen–acetylene ablation: (**a**) BP-0, (**b**) BP-5, (**c**) BP-10, (**d**) BP-15, and (**e**) BP-20.

Meanwhile, the microstructure of the ablated surface was observed as well (Figure 12). Obviously, there were serious and visible damages, such as holes and grooves, on the surface of the carbon fibers in composites without B_4C particles. The degree of oxidation of the carbon fibers was greatly relieved with increasing B_4C particles; that is to say, no obvious holes were observable in BP-10, BP-15 and BP-20.
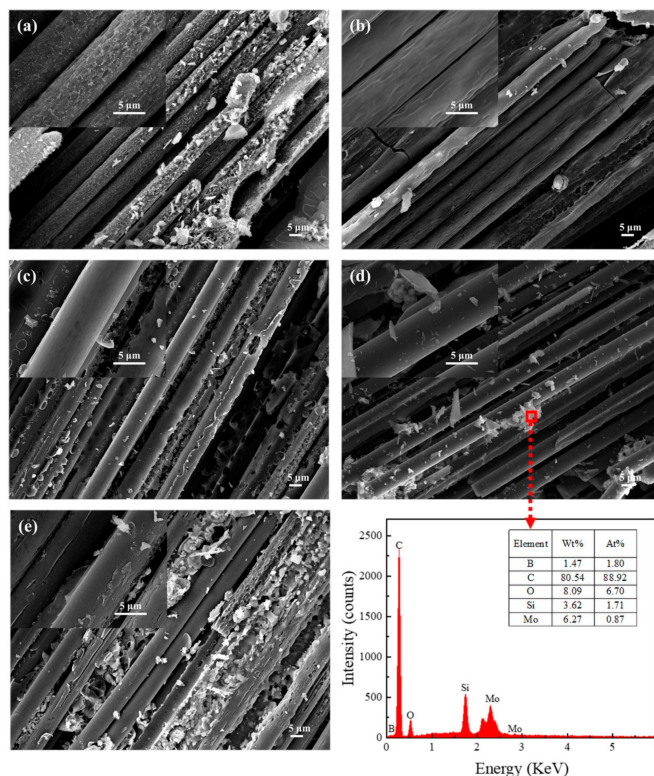
Figure 12. Micromorphology of the ablated surface for composites modified with different B$_4$C content: (**a**) BP-0, (**b**) BP-5, (**c**) BP-10, (**d**) BP-15, and (**e**) BP-20. EDS analysis of oxyacetylene ablation sample of BP-15.

3.6.3. Phase Composition of Ablated Surface

To further identify the phase compositions of the ablated surface, the residues scraped off the surface after ablation are subjected to phase analysis by the X-ray diffractometer, as shown in Figure 13. It can be observed that the surface residues of BP-0 were significantly different from those of BP-15. Except for the characteristic peaks of MoSi$_2$ that were introduced, the peaks of MoO$_2$ were observed in the XRD patterns of BP-0 and BP-15, which are mainly attributed to the oxidation of MoSi$_2$ during ablation (reaction (10)). In addition, there were characteristic peaks of MoO$_3$ in the XRD pattern of BP-15 (reaction (4)).
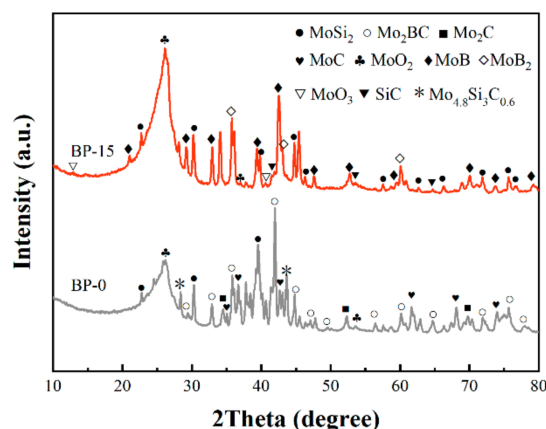
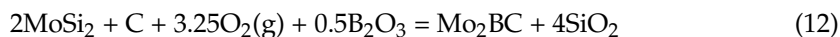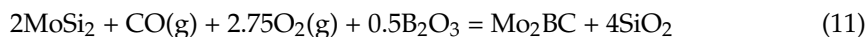$$MoSi_2 + 3O_2(g) = MoO_2 + 2SiO_2 \tag{10}$$

Figure 13. XRD patterns of residues from the ablated surface for BP-0 and BP-15.

The characteristic peaks of Mo_2BC, Mo_2C, MoC and $Mo_{4.8}Si_3C_{0.6}$ can also be seen in the XRD patterns of the BP-0 composites. Among them, Mo_2C and $Mo_{4.8}Si_3C_{0.6}$ were possibly formed by reaction (5) and reaction (6) respectively [47]. The reactions involved in the generation of Mo_2BC and MoC are as follows [42].

$$2MoSi_2 + CO(g) + 2.75O_2(g) + 0.5B_2O_3 = Mo_2BC + 4SiO_2 \tag{11}$$

$$2MoSi_2 + C + 3.25O_2(g) + 0.5B_2O_3 = Mo_2BC + 4SiO_2 \tag{12}$$

$$MoSi_2 + CO(g) + 1.5O_2(g) = MoC + 2SiO_2 \tag{13}$$

$$MoSi_2 + C + 2O_2(g) = MoC + 2SiO_2 \tag{14}$$

Besides the characteristic peaks of MoO_2 and MoO_3, the characteristic peaks of MoB, MoB_2 and SiC can also be seen in the XRD pattern of BP-15. A possible reason for this is that $MoSi_2$ undergoes oxidation reactions (4), (10) at a higher temperature, after which reactions (8), (9), (15), and (16) occur [48].

$$MoO_2 + 0.25B_4C + 1.75C = MoB + 2CO(g) \tag{15}$$

$$MoO_2 + 0.5B_4C + 1.5C = MoB_2 + 2CO(g) \tag{16}$$
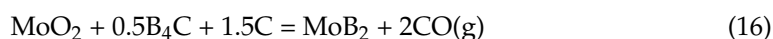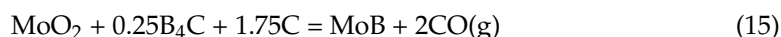
As for SiC, it was possibly derived from the reaction of SiO_2 and PyC [12,47].

$$SiO_2 + 3C = SiC + 2CO(g) \tag{17}$$

The thermodynamic parameters of the reactions involved in this paper are shown in Table A1.

3.7. Effect of MoSi₂ and B₄C on Carbon Fiber Oxidation in Composites

Combined with the above-mentioned results and discussions, $MoSi_2$ and B_4C particles possess a positive effect on carbon fiber an-oxidation in composites. On the one hand, $MoSi_2$ and B_4C particles can react with oxygen and other oxygen-containing gases, such as CO. In other words, $MoSi_2$ and B_4C particles consume a lot of oxygen around the composites, thus the oxidation reaction of carbon fibers in composites is mitigated. On the other hand, molten B_2O_3 derived from B_4C acts as an oxygen barrier so that an amount of oxygen can be blocked outside the composites, which mitigates the oxidation degree of carbon fibers in the composites as well. In addition, multiphase ceramics derived from $MoSi_2$, such as MoB, MoB_2, Mo_2C and $Mo_{4.8}Si_3C_{0.6}$, play the roles of oxygen barriers as well. Therefore, BP-15, which is composed of carbon fibers, boron phenolic resin and $MoSi_2$ and B_4C particles, exhibits excellent high temperature behavior.

4. Conclusions

In this work, the thermal stability, flexural strength, phase composition, microstructure, and ablation resistance of ceramizable composites were studied, and the oxidation behavior of carbon fibers in composite materials was demonstrated.

The results indicate that the incorporation of B_4C improves the performance of composites at high temperatures. TG-DTG shows that the residual weight rate of composites with 15 phr B_4C(BP-15) sufficiently increased from 23.03% to 32.91% compared with the composites without B_4C(BP-0). After being treated at 1400 °C for 15 min, the flexural strength of BP-15 increased by 17.79% compared with BP-0. The incorporation of B_4C particles effectively improved the ablation performance of the composites. Compared with BP-0, the line ablation rate and mass ablation rate of BP-15 were reduced by 53.96% and 1.56%, respectively. Compared with BP-0, the line ablation rate and mass ablation rate of BP-15 were reduced by 53.96% and 1.56%, respectively. In addition, $MoSi_2$ and B_4C particles have a positive effect on the oxidation of carbon fibers in composite materials. The oxidation degree of carbon fibers was greatly relieved with increasing B_4C particles.

After treatment at 1400 °C, the diameter of the as-received carbon fiber was reduced by 31.68%, while the diameter of carbon fiber in BP-0 and BP-15 decreased by 15.12% and 6.14%, respectively.

According to the morphology and XRD analysis of the composites, we found that $MoSi_2$-derived complex-phase ceramics (MoB, MoB_2, Mo_2C, $Mo_{4.8}Si_3C_{0.6}$, etc.) with high melting points were formed at high temperatures. Liquid B_2O_3 and $MoSi_2$-derived complex-phase ceramics played a role of an oxygen barrier, effectively mitigating the oxidation degree of the carbon fibers and enhancing the performance of composites at high temperatures.

Author Contributions: Conceptualization, T.Y., C.D. and M.S.; methodology, T.Y., C.D. and Z.D.; validation, Y.R., P.L. and P.H.; formal analysis, T.Y.; investigation, T.Y., C.D. and Y.R.; resources, Z.D. and C.D.; writing—original draft preparation, T.Y.; writing—review and editing, Z.D. and M.S.; visualization, T.Y.; supervision, Z.H.; project administration, Z.H. and M.S.; funding acquisition, M.S. All authors have read and agreed to the published version of the manuscript.

Institutional Review Board Statement: Not applicable.

Informed Consent Statement: Not applicable.

Data Availability Statement: The data presented in this study are available on request from the corresponding author.

Conflicts of Interest: The authors declare no conflict of interest.

Appendix A

Table A1. Thermodynamic parameters [2] of reactions.

Reaction	ΔG (kJ/mol)							
	800 °C	**1000 °C**	**1200 °C**	**1400 °C**	**1600 °C**	**1800 °C**	**2000 °C**	**2200 °C**
(3)	−4708.499	−4478.956	−4252.360	−4028.161	−3805.981	−3588.251	−3377.260	−3168.831
(4)	−1781.391	−1675.767	−1572.219	−1470.295	−1369.734	−1271.108	−1174.976	−1080.064
(5)	−344.272	−525.977	−703.651	−878.027	−1049.531	−1218.490	−1385.158	−1549.733
(7)	−144.394	−234.337	−322.212	−408.403	−493.150	−576.646	−659.053	−740.511
(8)	−242.457	−330.223	−415.840	−499.675	−581.943	−662.808	−742.401	−820.826
(9)	−206.397	−296.627	−385.521	−473.544	−560.980	−648.041	−734.887	−821.643
(10)	−1699.199	−1597.309	−1496.734	−1397.354	−1299.107	−1202.741	−1108.966	−1016.649
(13)	−1128.581	−1042.883	−957.937	−873.603	−789.778	−707.155	−626.376	−546.231
(14)	−1335.313	−1267.079	−1199.388	−1132.122	−1065.191	−999.301	−935.104	−871.398
(15)	−117.916	−184.486	−249.874	−314.098	−377.157	−439.029	−499.683	−559.075
(16)	−81.856	−150.890	−219.554	−287.967	−356.194	−424.262	−492.169	−559.892
(17)	240.864	173.222	106.285	39.969	−25.786	−90.633	−154.249	−217.232

[2]: Thermodynamic parameters come from the HSC Chemistry software.

References

1. Gnoffo, P.A. Planetary-Entry Gas Dynamics. *Annu. Rev. Fluid Mech.* **1999**, *31*, 459–494. [CrossRef]
2. Laub, B.; Venkatapathy, E. Thermal Protection System Technology and Facility Needs for Demanding Future Planetary Missions. In Proceedings of the International Workshop Planetary Probe Atmospheric Entry and Descent Trajectory Analysis and Science, Lisbon, Portugal, 6–9 October 2003; ESA Publications Division: Noordwijk, The Netherlands, 2004; Volume 544, pp. 239–247.
3. Davis, J.B.; Marshall, D.B.; Oka, K.S.; Housley, R.M.; Morgan, P.E.D. Ceramic Composites for Thermal Protection Systems. *Compos. Part A Appl. Sci. Manuf.* **1999**, *30*, 483–488. [CrossRef]
4. Deng, Z.; Yue, J.; Huang, Z. Solvothermal Degradation and Reuse of Carbon Fiber Reinforced Boron Phenolic Resin Composites. *Compos. Part B Eng.* **2021**, *221*, 109011. [CrossRef]
5. Mansouri, J.; Burford, R.P.; Cheng, Y.B. Pyrolysis Behaviour of Silicone-Based Ceramifying Composites. *Mater. Sci. Eng. A* **2006**, *425*, 7–14. [CrossRef]
6. Saghar, A.; Khan, M.; Sadiq, I.; Subhani, T. Effect of Carbon Nanotubes and Silicon Carbide Particles on Ablative Properties of Carbon Fiber Phenolic Matrix Composites. *Vacuum* **2018**, *148*, 124–126. [CrossRef]

7. Wang, S.; Huang, H.; Tian, Y.; Huang, J. Effects of SiC Content on Mechanical, Thermal and Ablative Properties of Carbon/Phenolic Composites. *Ceram. Int.* **2020**, *46*, 16151–16156. [CrossRef]

8. Song, J.; Huang, Z.; Qin, Y.; Wang, H.; Shi, M. Effects of Zirconium Silicide on the Vulcanization, Mechanical and Ablation Resistance Properties of Ceramifiable Silicone Rubber Composites. *Polymers* **2020**, *12*, 496. [CrossRef]

9. Chen, Y.; Chen, P.; Hong, C.; Zhang, B.; Hui, D. Improved Ablation Resistance of Carbon-Phenolic Composites by Introducing Zirconium Diboride Particles. *Compos. Part B Eng.* **2013**, *47*, 320–325. [CrossRef]

10. Ding, J.; Sun, J.; Huang, Z.; Wang, Y. Improved High-Temperature Mechanical Property of Carbon-Phenolic Composites by Introducing Titanium Diboride Particles. *Compos. Part B Eng.* **2019**, *157*, 289–294. [CrossRef]

11. Xu, F.; Zhu, S.; Ma, Z.; Liu, H.; Chen, Y.; Wu, T. Effect of TaSi2/ZrSi2 on Ablation Properties of Carbon-Phenolic Composite Irradiated by High-Intensity Continuous Laser. *Ceram. Int.* **2020**, *46*, 28443–28450. [CrossRef]

12. Yang, W.; Xu, B.; Qi, M.; Chen, D.; Ding, J.; Huang, Z.; Wang, Y. Improving Ablation Properties of Ceramifiable Vitreous Silica Fabric Reinforced Boron Phenolic Resin Composites via an Incorporation of $MoSi_2$. *Plast. Rubber Compos.* **2020**, *49*, 456–469. [CrossRef]

13. Yan, J.H.; Wang, Y.; Liu, L.F.; Wang, Y.; Chen, F. Preparation of Protective $MoSi_2$ Coating on Niobium Substrate. *J. Therm. Spray Technol.* **2015**, *24*, 1093–1099. [CrossRef]

14. Lohfeld, S.; Schütze, M. Oxidation Behaviour of Particle Reinforced $MoSi_2$ Composites at Temperatures up to 1700 °C Part I: Literature Review. *Mater. Corros.* **2005**, *56*, 93–97. [CrossRef]

15. Samadzadeh, M.; Oprea, C.; Karimi Sharif, H.; Troczynski, T. Comparative Studies of the Oxidation of $MoSi_2$ Based Materials: Low-Temperature Oxidation (300–900 °C). *Int. J. Refract. Met. Hard Mater.* **2017**, *66*, 11–20. [CrossRef]

16. Wang, L.; Fu, Q.G.; Liu, N.K.; Shan, Y.C. Supersonic Plasma Sprayed $MoSi_2$–ZrB_2 Antioxidation Coating for SiC–C/C Composites. *Surf. Eng.* **2016**, *32*, 508–513. [CrossRef]

17. Yong, X.; Cao, L.; Huang, J.; Kong, W.; Su, J.; Li, C.; Ouyang, H.; Zhou, L.; Liu, J. Microstructure and Oxidation Protection of a $MoSi_2$/SiO_2-B_2O_3-Al_2O_3 Coating for SiC-Coated Carbon/Carbon Composites. *Surf. Coatings Technol.* **2017**, *311*, 63–69. [CrossRef]

18. Zhang, P.; Chen, C.; Chen, Z.; Ren, X.; Shen, C.; Feng, P. Reaction Synthesis of Spark Plasma Sintered $MoSi_2$-B_4C Coatings for Oxidation Protection of Nb Alloy. *Ceram. Int.* **2019**, *45*, 4290–4297. [CrossRef]

19. Chung, D.D.L. *Carbon Fiber Composites [M]*; Butterworth-Heinemann: Oxford, UK, 1994; ISBN 978-0-08-050073-7.

20. Logesh, G.; Lodhe, M.; Balasubramanian, M. Effect of Temperature and Gaseous Medium on the Evolved Microstructures of Carbon Fiber Reinforced Reaction Bonded Silicon Nitride Composites. *Ceram. Int.* **2017**, *43*, 6110–6116. [CrossRef]

21. Che, D.; Saxena, I.; Han, P.; Guo, P.; Ehmann, K. Machining of Carbon Fiber Reinforced Plastics/Polymers: A Literature Review. *J. Manuf. Sci. Eng.* **2014**, *136*, 34001. [CrossRef]

22. Huang, Z.; Deng, Z.; Dong, C.; Fan, J.; Ren, Y. A Closed-Loop Recycling Process for Carbon Fiber Reinforced Vinyl Ester Resin Composite. *Chem. Eng. J.* **2022**, *446*, 137254. [CrossRef]

23. Xiang, Y.; Li, X.; Du, A.; Wu, S.; Shen, J.; Zhou, B. Timing of Polyethylene Glycol Addition for the Control of SiO_2 Sol Structure and Sol–Gel Coating Properties. *J. Coat. Technol. Res.* **2017**, *14*, 447–454. [CrossRef]

24. Xia, K.; Lu, C.; Yang, Y. Preparation of Anti-Oxidative SiC/SiO_2 Coating on Carbon Fibers from Vinyltriethoxysilane by Sol–Gel Method. *Appl. Surf. Sci.* **2013**, *265*, 603–609. [CrossRef]

25. Kim, G.; Lee, H.; Kim, K.; Kim, D.U. Effects of Heat Treatment Atmosphere and Temperature on the Properties of Carbon Fibers. *Polymers* **2022**, *12*, 2412. [CrossRef] [PubMed]

26. Kwon, Y.J.; Kim, Y.; Jeon, H.; Cho, S.; Lee, W.; Lee, J.U. Graphene/Carbon Nanotube Hybrid as a Multi-Functional Interfacial Reinforcement for Carbon Fiber-Reinforced Composites. *Compos. Part B Eng.* **2017**, *122*, 23–30. [CrossRef]

27. Ribeiro, L.; Flores, O.; Furtat, P.; GERVAIS, C.; Kempe, R.; Machado, R.; Motz, G. A Novel PAN/Silazane Hybrid Polymer for Processing of Carbon-Based Fibres with Extraordinary Oxidation Resistance. *J. Mater. Chem. A* **2016**, *5*, 720–729. [CrossRef]

28. Wang, J.; Lin, W.; Wu, X.; Yang, Y.; Wu, F.; Yan, X. Preparation and Oxidation Behavior of a Double-Layer Coating for Three-Dimensional Braided Carbon Fiber. *Surf. Coat. Technol.* **2016**, *298*, 58–63. [CrossRef]

29. Xu, F.; Zhu, S.; Ma, Z.; Liu, Y.; Li, H.; Hu, J. Improved Interfacial Strength and Ablation Resistance of Carbon Fabric Reinforced Phenolic Composites Modified with Functionalized $ZrSiO_4$ Sol. *Mater. Des.* **2020**, *191*, 108623. [CrossRef]

30. Duan, L.; Zhao, X.; Wang, Y. Effects of Polycarbosilane Interface on Oxidation, Mechanical, and Ablation Properties of Carbon Fiber-Reinforced Composites. *Ceram. Int.* **2018**, *44*, 22919–22926. [CrossRef]

31. Zou, Z.; Qin, Y.; Fu, H.; Zhu, D.; Li, Z.; Huang, Z. ZrO2f-Coated Cf Hybrid Fibrous Reinforcements and Properties of Their Reinforced Ceramicizable Phenolic Resin Matrix Composites. *J. Eur. Ceram. Soc.* **2021**, *41*, 1810–1816. [CrossRef]

32. Yang, G.; Yang, G.; Wang, W.; Peng, S.; Huang, Z. The Research on Oxidation Resistance Ability and Mechanical Properties of Carbon Fiber Reinforced Phenolic Resin Composites. *Mater. Res. Express* **2020**, *7*, 065604. [CrossRef]

33. Ding, J.; Yang, T.; Huang, Z.; Qin, Y.; Wang, Y. Thermal Stability and Ablation Resistance, and Ablation Mechanism of Carbon–Phenolic Composites with Different Zirconium Silicide Particle Loadings. *Compos. Part B Eng.* **2018**, *154*, 313–320. [CrossRef]

34. Wang, S.; Wang, Y.; Bian, C.; Zhong, Y.; Jing, X. The Thermal Stability and Pyrolysis Mechanism of Boron-Containing Phenolic Resins: The Effect of Phenyl Borates on the Char Formation. *Appl. Surf. Sci.* **2015**, *331*, 519–529. [CrossRef]

35. Trick, K.A.; Saliba, T.E. Mechanisms of the Pyrolysis of Phenolic Resin in a Carbon/Phenolic Composite. *Carbon N. Y.* **1995**, *33*, 1509–1515. [CrossRef]

36. Chen, X.; Li, S.; Yan, L.; Yuan, Y. Curing and Pyrolysis of Boron-Modified Phenolic Resin. *Fuhe Cailiao Xuebao/Acta Mater. Compos. Sin.* **2011**, *28*, 89–95.

37. Hatami Ramsheh, H.; Faghihi Sani, M.A.; Kokabi, A.H. Microstructure and Mechanical Properties of MoSi$_2$–MoSi$_2$ Joints Brazed by Ag–Cu–Zr Interlayer. *Mater. Des.* **2013**, *49*, 197–202. [CrossRef]

38. Zhu, L.; Wang, X.; Ren, X.; Kang, X.; Akhtar, F.; Feng, P. Preparation and High-Temperature Oxidation Resistance of Multilayer MoSi$_2$/MoB Coating by Spent MoSi$_2$-Based Materials. *J. Am. Ceram. Soc.* **2021**, *104*, 3682–3694. [CrossRef]

39. Gnesin, B.A.; Gnesin, I.B.; Nekrasov, A.N. The Interaction of Carbon with Mo$_5$Si$_3$ and W$_5$Si$_3$ Silicides. Nowotny Phase Synthesis. *Intermetallics* **2013**, *41*, 82–95. [CrossRef]

40. Gao, P.; Xu, M.; Xie, W.; Lü, H.; Li, Q.; Peng, S.; Xiao, H. Study on Formation Mechanism of Mo$_{4.8}$Si$_3$C$_{0.6}$ Nanopowders Prepared by Solid-Reaction Method. *Hunan Daxue Xuebao/J. Hunan Univ. Nat. Sci.* **2018**, *45*, 85–89. [CrossRef]

41. Lee, D.B.; Woo, S.W. Oxidation of SiOC Composite Having Dispersoids of Mo$_{4.8}$Si$_3$C$_{0.6}$ and MoSi$_2$. *Mater. Sci. Forum* **2005**, *486–487*, 165–168. [CrossRef]

42. Kumar, S.; Sairam, K.; Sonber, J.K.; Murthy, T.S.R.C.; Reddy, V.; Nageswara Rao, G.V.S.; Srinivasa Rao, T. Hot-Pressing of MoSi$_2$ Reinforced B4C Composites. *Ceram. Int.* **2014**, *40*, 16099–16105. [CrossRef]

43. Paul, A.; Venugopal, S.; Binner, J.G.P.; Vaidhyanathan, B.; Heaton, A.C.J.; Brown, P.M. UHTC-Carbon Fibre Composites: Preparation, Oxyacetylene Torch Testing and Characterisation. *J. Eur. Ceram. Soc.* **2013**, *33*, 423–432. [CrossRef]

44. Feng, T.; Li, H.; Hu, M.; Lin, H.; Li, L. Oxidation and Ablation Resistance of the ZrB$_2$-CrSi$_2$-Si/SiC Coating for C/C Composites at High Temperature. *J. Alloys Compd.* **2016**, *662*, 302–307. [CrossRef]

45. Tang, S.; Deng, J.; Wang, S.; Liu, W.; Yang, K. Ablation Behaviors of Ultra-High Temperature Ceramic Composites. *Mater. Sci. Eng. A* **2007**, *465*, 1–7. [CrossRef]

46. Zhao, D.; Zhang, C.; Hu, H.; Zhang, Y. Ablation Behavior and Mechanism of 3D C/ZrC Composite in Oxyacetylene Torch Environment. *Compos. Sci. Technol.* **2011**, *71*, 1392–1396. [CrossRef]

47. Feng, Y.; Yang, Y.; Wen, Q.; Riedel, R.; Yu, Z. Dielectric Properties and Electromagnetic Wave Absorbing Performance of Single-Source-Precursor Synthesized Mo$_{4.8}$Si$_3$C$_{0.6}$/SiC/C$_{free}$ Nanocomposites with an in Situ Formed Nowotny Phase. *ACS Appl. Mater. Interfaces* **2020**, *12*, 16912–16921. [CrossRef]

48. Tian, X.D.; Guo, X.P.; Sun, Z.P.; Qu, J.L.; Wang, L.J. Oxidation Resistance Comparison of MoSi2 and B-Modified MoSi$_2$ Coatings on Pure Mo Prepared through Pack Cementation. *Mater. Corros.* **2015**, *66*, 681–687. [CrossRef]